NUMERICAL STUDY ON THE PHYSICS OF FLUID FLOW ABOUT A SAVONIOUS ROTOR

Placide Jaohindy, François Garde and Alain Bastide

Laboratoire de Physique et Ingénierie Mathématique appliquée à l'Energie et à l'EnvironnemeNT (PIMENT), Campus universitaire sud, Université de La Réunion, 117 Avenue du Général Ailleret, 97430, Le Tampon, France

ABSTRACT

This study reports the flow physics past a Savonious wind turbine rotor. It is based on the modeling and numerical simulation of a VAWT experiments. The computational fluid dynamics (CFD) techniques was used with a rigid-rotor system to model the coupling. The SST k-ω model is the turbulence model taken into account in this dynamic study of a Savonious rotor. The rotor motion was governed by a 1-DOF method. The physics of the fluid flow in and around the Savonious rotor was analyzed by the velocity, pressure and vorticity fields induced by the rotor rotation. It is founded that the half-period of formation and destruction of vortices generated by the Savonious rotor is between 90 deg to 270 deg.

1. Introduction

The Savonious rotor is a vertical axis wind turbine (VAWT) originally invented by a Finnish engineer Sigurd J. Savonius in 1922 and its concept is based on the principle developed by Flettner [1, 2]. Like other wind turbines, the Savonious rotor operation depend on the wind velocity and its geometrical parameters. The harmonic motion of this rotor come from the existence of a single plane of symmetry along its rotational axis Oz. The Savonious rotor is a low power and slow running VAWT that starts at low wind speed of 2 to 3 m/s. The advantage of this rotor is he accept wind from any directions without orientations. Many investigations were undertaken in the past to identify the aerodynamic parameters of this wind turbine. The efficiency of the Savonius rotor originel is 20%. The conventional Savonius rotor can reach a power coefficient Cp of 30% with a static torque coefficient of 33%. The overlap ratio β=e/d of this rotor is between 0.2 to 0.3 [13]. Blackwell et al. (1977) studied the performance of fifteen configurations of a Savonious rotor in wind tunnel conditions [4]. They make vary the dynamic torque coefficient Ct and the power coefficient Cp of the rotor functions of the tip speed ratio λ, the overlap ratio β and the Reynolds number Re during their study. The Cp obtained by the three-blade Savonious rotor was 0.18 for β=0.10. For the same β, the maximum of Ct obtained with two blades Savonious rotor is 0.35. They pointed out that the increase of the Re number increase the performance of the Savonious rotor.

The important parameters of a VAWT motion is the inertial parameters J and its aerodynamic shape. The equations of motion of this VAWT allowed to find more informations about the flow physics passing through the Savonious rotor. The wind turbine rotor flow analysis is an important study must be undertaken before sizing the wind turbine itself. The vortices generated by the Savonious rotor rotation reduce significantly the energy captured by its blades. To clarify the effect of the overlap ratio β on the flow mechanism, Fujisawa studied the flow fields in and around Savonious rotors at various β in a water chanel. He compared his experimental results with a two-dimensional numerical study using the discrete vortex method [8]. Fujisawa concluded that the two-dimensional simulation approach of the flow is not valid and the numerical study of a Savonious rotor had to be conducted in a three-dimensional approach to have a better representation of the three-dimensional vortical structure around the rotor [8]. The importance of the three-dimensional properties of the fluid flow in a case of a Savonious rotor led us to conduct this study in three-dimensions.

The purpose of this paper is first to provide a brief overview of a steady and unsteady computational strategies to validate our simulation. A variable speed is an interesting approach to recreate the real Savonious rotor motion. Next, the governing equations of the incompressible fluid and the Savonious rotor will be concisely presented. This unsteady problem has been conducted with the SST k-ω model. Finally, the dynamic study has permitted to study the dependency analysis between velocity-pressure and vorticity fields generated by the VAWT rotation.

2. Numerical method

RANS solver for incompressible flow was used with the SST k-ω approach, because these models have a rapid convergence with interesting results. The three-dimensional RANS equations were discretized in the computational domain by a finite volume method. The time integration was accomplished by the Euler implicit scheme. This integration gives a temporal variation of unsteady parameters of the simulation using 1-DOF method. By applying the Reynolds decomposition in a tensor form, the conservation equations of continuity and momentum in steady state are given by the following relations:

$$\frac{\partial U_j}{\partial x_j} = 0 \qquad \text{(eq.1)}$$

$$\frac{\partial U_i}{\partial t} + \frac{\partial}{\partial x_j}(U_i U_j) = -\frac{1}{\rho}\frac{\partial p}{\partial x_i} + \frac{\partial}{\partial x_j}\left[\nu\left(\frac{\partial U_i}{\partial x_j} + \frac{\partial U_j}{\partial x_i}\right) - \overline{u_i' u_j'}\right] \qquad \text{(eq.2)}$$

The term $\overline{u_i' u_j'}$ represents the Reynolds stresses. It allows taking into account the turbulence phenomenon. In this study, the SST k-ω model is used. The SST k-ω is an hybrid model based on the standard k-ε and k-ω models and developed by Menter [12]. The standard k-ε model is also called the two equations model and derived from the linear eddy viscosity model. With the standard k-ε model approach, two transport equations are used to solve the Reynolds stress tensor [10]. These two equations are respectively, the transport equation for the kinetic energy k and the dissipation rate ε. The standard k-ε model suits well for a turbulent flow far from the walls [10]. The first Menter's interest was to improve the performances for adverse pressure gradient (APG) flows and the second was to solve the problem of spurious sensitivity to free-stream conditions [14]. Christopher et al. (2002) argued that the k-ω model performed poorly for wall bounded separated flows caused by the APG [7].

2. Computational domain and mesh

The computational domain used in this study at Fig. 1 is a parallelepiped, with a size of (20 meters × 10 meters × 3 meters) and has two regions. A cylinder of one meter radius and three meters height is placed at the center of this domain. The Savonious rotor is interdependent to the cylindrical region and placed at one point five meter high along the rotational axis Oz. With the steady state simulation, the wind turbine rotor was moved manually by rotating the internal region. The parallelepiped and the cylinder are centered at (0, 0, 1) meter. The Savonious rotor is centered at (0, 0, 1.5) meter. In the unsteady simulation, the internal region motion was imposed by the angular velocity ω of the rotor. The Savonious rotors, the external and internal regions of the computational domain are modeled with polyhedral elements.

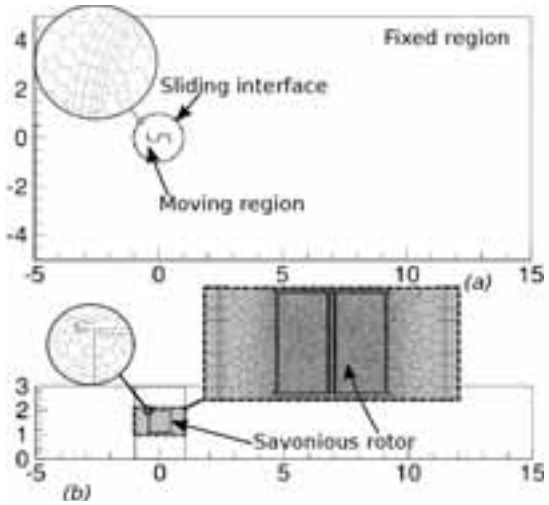

Fig. 1: The computational domain used in this present study. The Savonious rotor is positioned at the half of the domain. The dimension of the radius of the internal region is 2.22R. The wind flow direction at the computational domain is along the Ox axis.

The computational domain is composed of 61, 198 cells and the minimum polyhedral cells width of this domain near the wind turbine rotor is equal to 0.015 meter. The computational domain of the dynamical study includes 242, 198 cells and has minimum polyhedral cells width of 0.0074 meter. The Savonious rotor cells were refined compared to the average computational domain cells size. The quality of simulation results depends on the quality of the rotor and computational domain mesh. For a Savonious rotor height H=1 meter, the computational domain cells Δx of the rotor cells is 0.015 meter. The Δx of the computational domain cells are 0.0047 meter and will be used to calculate the time step Δt of the unsteady simulation.

2.1. Geometry of the rotor

The Savonious rotor used in this study in Fig. 2a and 2b has the following features: height H = one meter, radius R=0.4512 meter, β=0.2 and a=0. Before the Savonious rotor of Ushiyama and Nagai [13], the Savonious rotors of Blackwell et al. (1977) are the most studied low efficiency wind turbine [4]. The Savonious rotor of Run 35 and Run 37 of Blackwell et al. (1977) was used because the uncertainty analysis of the dynamic torque coefficient Ct and the power coefficient Cp curves of this rotor was measured in their experiments [4]. The thickness ep of the Savonious rotor is not mentioned in their manuscript but a ep of 0.0021 meter was used after a several tests. We tested the following values of ep: 0.01 meter, 0.005 meter, 0.003 meter and 0.0021 meter. We founded that 0.0021 meter is a reasonable thickness of the Savonious rotor for the dynamic study. A Savonious rotor with ep=0.0021 meter give Ct and Cp gives modeling results very close to the experiment results. The steady studies of the Savonious rotor are independent of the thickness of the rotor and a ep in range of 0.01 to 0.0021 meters are considered. For the steady state study, ep=0.01 meter was chosen.

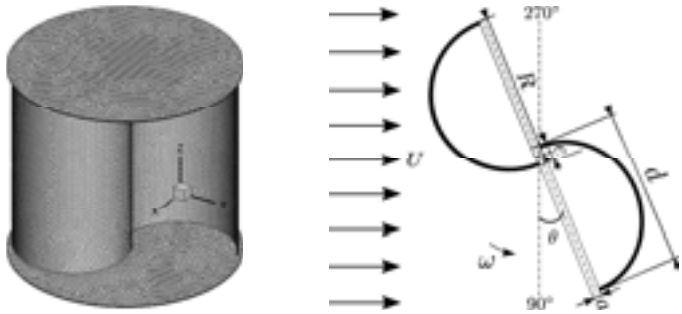

Fig. 2: Sketch and geometric parameters of the Savonious rotor. Polyhedral cells sizes are uniform for the blades and endpaltes of the Savonious rotor. For the height H=one meter, the minimal Savonious rotor cells thickness Δx was 0.015 meter. Θ=0 deg was the initial position of the Savonious rotor take into account in this study.

2.2. Boundary conditions

To set up this study, we had to determine the thermophysical properties of air at the experiments. Knowing Re, we estimated the ρ and μ of the air. For a Re of 4.32×105 we founded that ρ=1.2157 kg/m3 and μ=1.777×105 Ns/m^2. The exact value of ρ and μ of the air is necessary to solve the incompressible CFD problem. The variation of these two parameters affects the numerical simulation results. The inlet boundary conditions include the free stream velocity U=7 m/s at Re=4.32×10^5. Pressure outlet boundary conditions specify the static pressure at flow outlets. The outlet boundary is far enough from the rotor with a constant static pressure which can be measured experimentally. A symmetry plane was used for the top, lower, left and right parts of the computational domain. The Savonious rotor was manufactured using aluminum with a ρ of 2700 kg/m3. The Mr=17.74 kg and IOz=2 kgm^2 was estimated analytically.

2. Resolution methods

In this section, the aerodynamic parameters and the formulation of the equations of motion of the wind turbine was presented. Only the component of inertia matrix JOz along Oz axis was considered in the simulation with the axial symmetry of the rotor. The relationship between the time step Δt and the minimal length of the domain cells Δx was presented. This present study was performed by using a CFD solver with steady and unsteady simulations capabilities [5]. The Savonious rotor motion resolution is obtained by a fluid rigid-rotor method. The CFD method can be used to conduct an unsteady simulation with implicit or explicit schemes. The implicit scheme was used for the unsteady simulation because the implicit methods have a better convergence than the explicit method.

The dynamic torque coefficient Ct and the power coefficient Cp developed by the VAWT is given by the following expressions:

$$C_t = \frac{M_t}{\frac{1}{2}\rho DAU^2} \quad \text{(eq.3)}$$

$$C_p = \frac{M_t \omega}{\frac{1}{2}\rho AU^3} \quad \text{(eq.4)}$$

Where A is the projected area of the rotor, D is the diameter of the rotor, U is a free stream velocity. M is the output of the steady simulation. Θ, ω and Mt are the output of the unsteady strategies. The aerodynamic power P acting on the Savonious rotor blades is given by $M_t\omega$.

2.1. Equation of motion of the Savonious rotor

The Savonious rotor motion was considered as a rigid-rotor rotation around a fixed axis Oz. The equation of motion of the rotor is a second order differential equation and its expression is given by the following equation:

$$I_{Oz}\ddot{\theta} = M_{Oz} + G_{Oz} \quad \text{(eq.5)}$$

Where IOz is the component of the matrix J along Oz axis. MOz is the moment of forces acting on the Savonious rotor. GOz represents the external forces acting on the Savonious rotor. Assuming that the Savonious rotor makes a perfect pivot with his rotational axis Oz, this implies that GOz is equal to zero. The equation of motion of the Savonious rotor is then:

$$I_{Oz}\ddot{\theta} = M_{Oz} \quad \text{(eq.6)}$$

Where Mp is the pressure moments, Mτ is the viscous stress moment, Mf is the external forces moment. fr is the ramping factor and it was applied to MOz and GOz on the body and used to minimize the shock caused by the coupling between structural and fluid dynamics [5]. The specificity of the dynamic study compared to the steady study is the taking into account of the inertia of the rotor characterized by J. Eq. (6) of the rigid-rotor is then solved at each time step Δt [5].

3. Results and discussions

3.1 Unsteady study of the Savonious rotor

The unsteady study of the Savonious rotor gives power coefficient Cp and dynamic torque coefficient Ct curves in Fig. 2a and 2b. These figures are obtained by the superpositions of several equilibrium states of the rotor. To define these curves, we carried out simulations in a range of external forces moments Mf in Tab. 1.

Tab. 1: Summary of data obtained from the dynamic study of the Savonious rotor with the SST k-ω model.

Mf(Nm)	λ	Mt(Nm)	ω(rad/s)	P(W)	Δt(s)
-4.2	0	4.12	0	0	0.02
-4.0	0	4.12	0	0	0.001
-3.95	0.19	4.44	2.83	12.35	0.001
-3.9	0.57	4.57	8.84	40.41	0.001
-3.6	0.69	3.70	10.71	39.61	0.001
-3.0	0.85	2.65	13.19	39.56	0.0005
-2.6	0.95	2.65	14.75	39.10	0.0005
-2.0	1.11	2.00	17.22	34.44	0.0005
-0.1	1.54	0.28	23.89	6.69	0.0004

At each unsteady simulation, the angular velocity ω of the rigid-rotor in Fig. 5 starts at 0 rad/s before reaching its equilibrium state. Each rigid-rotor equilibrium state corresponds to a specific ω. The time step Δt was fixed by the experimental dynamic torque coefficient data. The number of iterations at each Δt was set at 20 and the sub-iteration number for the 1-DOF solver must be greater than 10 to attest the residuals convergence. The stopping criterion for each simulation was fixed at $10^{-}6$. The Δt is a parameter which intervenes in the modeling of the rigid-rotor motion. This choice is based on the compromise between accuracy and the simulation time T. A highest Δt may compromise the validity of results. A low Δt increases computing resources. The ω of the rigid-rotor during transitory state and at the equilibrium state was imposed by the Eq. (6). The ω and the dynamic torque Mt curves of the rigid-rotor corresponding to moment of external forces Mf=2.6 Nm are shown in the following Figure 5. At T =0 s, the rigid-rotor was positioned at 0 deg and beyond this time, it start moving and as T increases, the ω and Mt parameters tends to a stable average values at their equilibrium states.

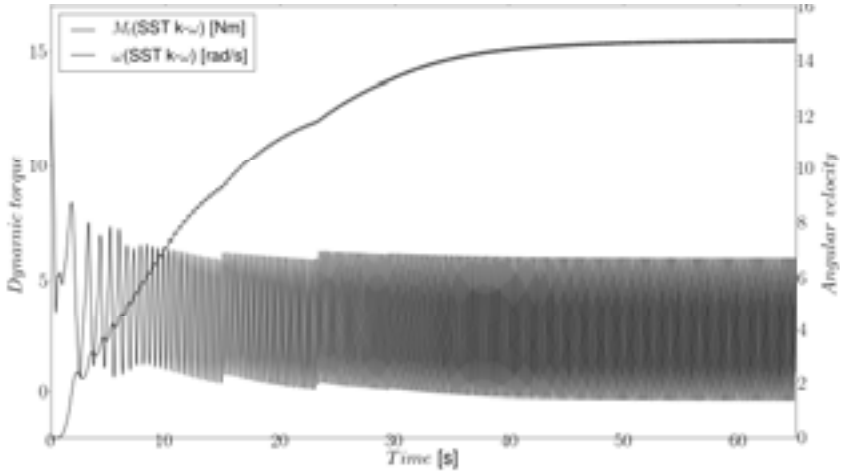

Fig. 5: Time-dependent dynamic torque and angular velocity of the Savonious rotor

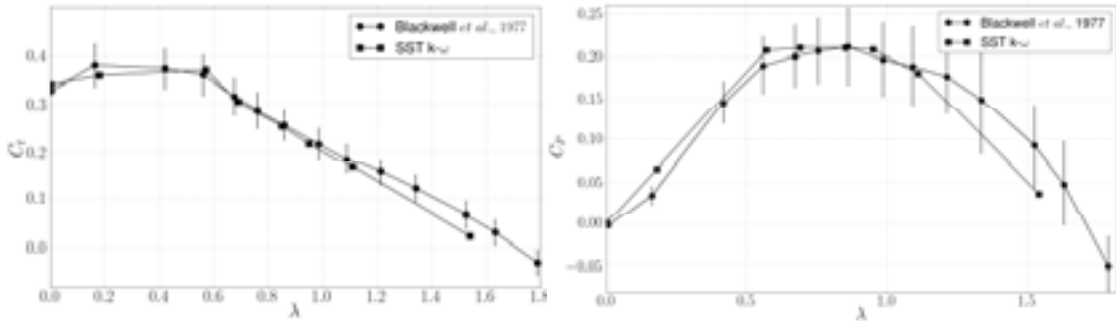

(a) (b)

Fig. 6: Tip speed ratio depending on the dynamic torque and power coefficients of the Savonious rotor.

Fig. 6 describe the dynamic torque coefficient Ct and the power coefficient Cp of a Savonious rotor in the range of moment of external forces Mf between -4.2 to -0.1 Nm depending on the tip speed ratio λ. Between Mf of -4 Nm to -3.8 Nm, the SST k-ω model is in agreement the Blackwell et al. (1977) curve with a small perturbation on the point corresponding to Mf=-3.9 Nm [4]. From λ=1.2 to the end, the SST k-ω model curve underestimate the Blackwell et al. (1977) curve [4]. In this range of λ, the dynamic torque coefficient Ct in Fig.6a curve get out the margin of error. If we analyze the data in Tab. 1, it was found that the SST k-ω model predict the rotor behavior accurately.

The power coefficient Cp in Fig.6b is an important parameter in a wind turbine study and it contribute in the wind turbine design. A Savonious rotor is often designed for a tip speed ratio λ near 1 [11]. The optimum λ obtained by the present study turn around 0.86. The SST k-ω model and the Blackwell et al. (1977) curves are close and have a common maximum of 0.21[4]. From λ=0 to 1, the standard k-ε and the SST k-ω models curves overestimate slightly the Blackwell et al. (1977) curve but they remains in the uncertainty intervals except at λ=0.21 [4]. From λ=1 to 1.47, the SST k-ω model curve underestimate the Blackwell et al. (1977) curve but it remains in the uncertainty intervals [4]. At λ maximal of 1.54, the Cp and the dynamic torque coefficient Ct curves obtained with this model overestimate tolerably the margins of error. The Figure 7 and 8 inform that the Ct and Cp curves obtained are in agreement with the experimental results.

2. Analysis of the flow field

In operation, the Savonious rotor generates a complex flow. Chauvin et al.(1983) argued that in their experiments in a water chanel for this rotor, the retracting blade generates a turbulent wake and the advancing blade is the seat of an intense trailing edge vortex rotating in the same direction of the rotor [3, 6]. They also precised that the motive vortices occur twice per revolution [6]. Analyzing the physics of flow over the Savonious rotor revolution, it was deduced that the preconisation of Chauvin et al. (1983) are consistent with the numerical simulation of the vortex formation in and around the rotor. For this constatation, the fluid flow study in this paper is restricted on a half-turn of the rotor. Fig. 7a shows the velocity field around a Savonious rotor taken at angle Θ=90 deg with a stagnation point at extrados of the retracting blade. The $\lambda 2 < 0$ criterion of Jeong and Hussain, 1995 is the vortices analysis and visualization method used here and at this position, the emptying of the advancing blade vortices is started [9]. This phenomenon is perceived in Fig. 7c where the fluids expelled from the intrados of the advancing blade created a low pressure area at the trailing edge of the blade. This phenomenon has already studied by Aouachria and he describes that it is a result of the pressure drop between the intrados and extrados at blade tip [2]. This phenomenon is accentuated in Fig. 7d where the Savonious rotor position Θ =123 deg and because the intrados of the advancing blade is in quite exposed to the wind incidence. The importance of this fact is perceived in Fig. 7f by expanding the diameter of the low pressure zone at the trailing edge of the advancing blade. In Fig. 9g where Θ=202 deg, the Savinous rotor tends to return to Θ=90 deg and the wind velocity streamline at the rotor plane is almost identical to those in Fig. 9a. After Θ=180 deg, the functionalities of the Savonious rotor blades was reversed. The advancing blade becomes the retracting blade and the retracting blade becomes the advancing blade.

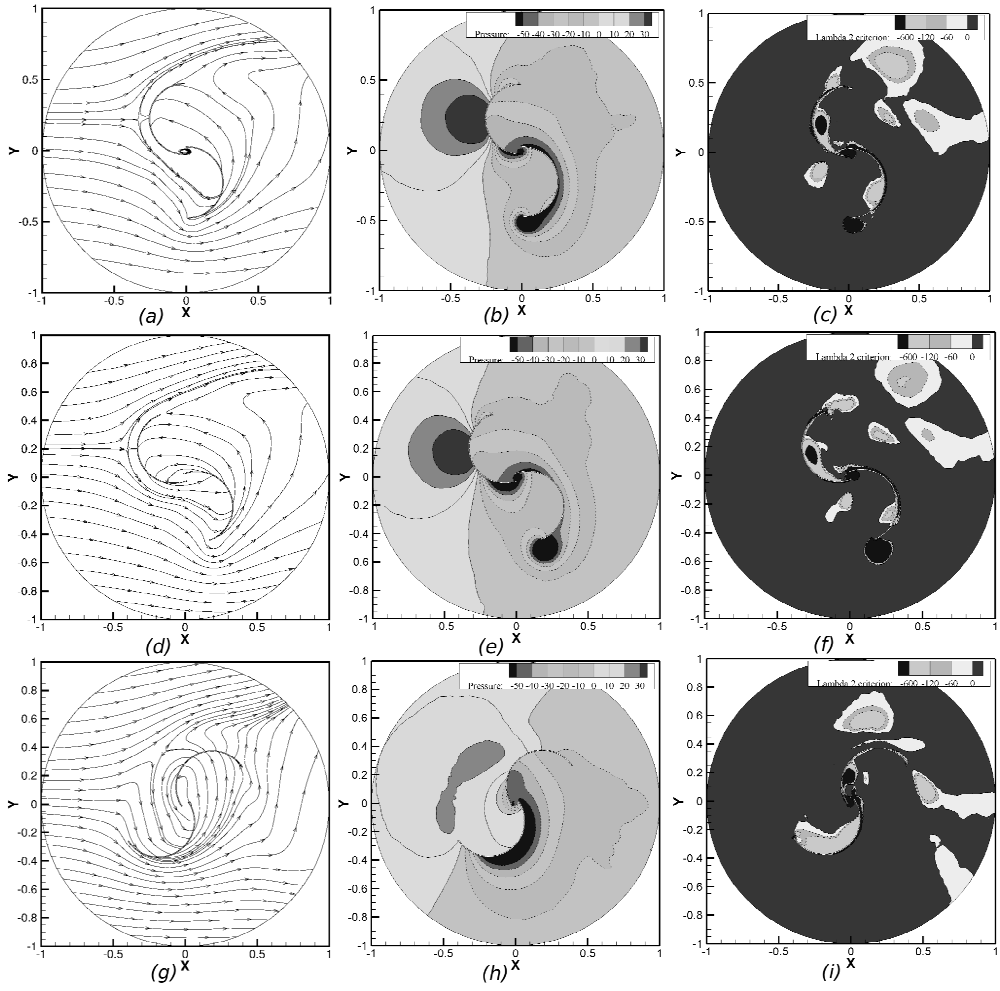

Fig. 7: Visualisation of the velocity, pressure and vorticity fields on a symetry plane of the Savonious rotor. The Savonious rotor positions was taken at λ of 90 deg, 123 deg and 202 deg. The method of Jeong and Hussain ($\lambda 2 < 0$) was used for the vorticity fields visualization.

After analysis of the vortex generated by the Savonious rotor, we propose that the swirling zone in and around the rotor come partly from the low pressure formed by the vacuum created by the shear stress during its rotation. The Fig. 8 brings more accuratelly to the emptying phenomenon in Fig. 7c and f. Fig. 8 also

shows vorticity fields through the Savonious rotor filtered with λ2=-600. This restriction enabled us to have a better visualisation of the swirling zone generated by the rotor in three-dimensions. Due to the axial symmetry of the Savonious rotor, the vortices generated at the upper part and the lower part of this rotor is identical.

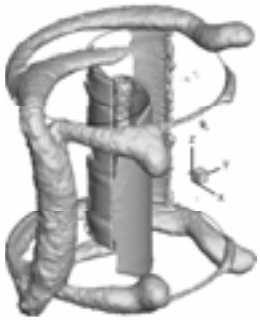

Fig. 8: Visualization of vorticity fields in and around the Savonious rotor in three-dimensional with the Jeong and Hussain's technique (λ2=-600).

2. Conclusions

A a three-dimensional CFD model of a Savonious rotor has been developed in this study. The model has been validated in unsteady state by comparison with experimental results. The numerical models used are based on the Navier Stokes equations with SST k-ω models. The results of the unsteady simulations of the Savonious rotor pointed out that the SST k-ω allow to predict a best approximation of the dynamic torque coefficient and the power coefficient of the Savonious rotor. The dynamic study had permit to study the fluid flow in and around the Savonius rotor thanks to the Jeong and Hussain technique. A link between velocity, pressure and vorticity fields has been identified. The analysis of the airflow through the Savonious rotor pointed out that the half-period of the formation and destruction of vortices generated by the rotor blades is in the range of Θ=90 deg to 270 deg. Due to the axial symmetry of the Savonious rotor, coherents structures has been observed at the upper and lower parts of the rotor.

References

[1] Ahuja, V., 2008. Optimization of fuel-air mixing for a scramjet combustor geometry using CFD and genetic algorithm. PhD Thesis, the Graduate Faculty of Auburn University.

[2] Aouachria, Z., 1987. Eolienne Savonious comportement mécanique et aérodynamique. PhD thesis, Université de provence.

[3] Béguier, C., Bousgarbiès, J. L., Leweke, T., 2001. Tourbillon, instabilité et décollement, Toulouse: Cépaduès, France.

[4] Blackwell, Ben F., Sheldahl Robert, E., Feltz Louis, V., 1977. Wind Tunnel Performance Data for TWO-and Three-Bucket Savonius Rotors. SAN D76-0131.

[5] CD-adapco. 2009. USER GUIDE : STAR-CCM+. Version 4.04.011.

[6] Chauvin, A., Botrini, M., Beguier, C., Brun, R., 1983. Evolution du coefficient de puissance d'un rotor Savonius. C. R. Acad.Sci. Paris. 296, 823-825.

[7] Christopher, L. R., Susan, X. Y., 2002. Prediction of high lift: review of present CFD capability. Progress in Aerospace Sciences. 38, 145-180.

[8] Fujisawa, N., 1996. Velocity measurements and numerical calculations of flow fields in and around Savonius rotors. Journal of Wind Engineering and Industrial Aerodynamics. 59, 39-50.

[9] Jeong, J., Hussain, F., 1995 On the Identification of a Vortex. J. Fluid Mechanics. 285, 69-94.

[10] Launder, B. E., Spalding, D. B., 1974. The numerical computation of turbulent flow. Computer Methods in Applied Mechanics and Engineering. 3, 269-289.

[11] Le Gourières D. Energie éolienne, théorie, conception et calcul pratique des installations. Eyrolles, Paris, France, 1982.

[12] Menter, F. R., 1994. Two-equation eddy-viscosity turbulence models for engineering applications. AIAA J. 32, 1598-1605.

[13] Ushiyama I., H., Nagai., 1988. Optimum design configurations and performances of Savonius rotors. Wind Eng.12, 59-75.

[14] Yorke, C. P., Coleman, G. N., 2004. Assessment of common turbulence models for an idealised adverse pressure gradient flow. European journal of mechanics. 23, 319-337.